Ex Situ Dissolution of CO2: A New Engineering Methodology Based on Mass-Transfer Perspective for Enhancement of CO2 Sequestration

ARTICLE *in* ENERGY & FUELS · JUNE 2011

Impact Factor: 2.79 · DOI: 10.1021/ef200199r

4 AUTHORS, INCLUDING:

Yuri Leonenko
University of Waterloo
26 PUBLICATIONS **250** CITATIONS

SEE PROFILE

energy&fuels

ARTICLE

pubs.acs.org/EF

Ex Situ Dissolution of CO_2: A New Engineering Methodology Based on Mass-Transfer Perspective for Enhancement of CO_2 Sequestration

Sohrab Zendehboudi,*[,†] Asif Khan,[†] Stephen Carlisle,[†] and Yuri Leonenko[‡]

[†]Department of Chemical Engineering, and [‡]Department of Physics and Astronomy, University of Waterloo, Waterloo, Ontario N2L 3G1, Canada

ABSTRACT: A new methodology is proposed for the acceleration of CO_2 dissolution to lower the risk of CO_2 leakage for carbon capture and storage (CCS) technology. It is called *ex situ* dissolution because CO_2 is being dissolved at a surface before it is injected underground. This new approach reduces or eliminates possible leakage of CO_2 from underground formation. To achieve full underground dissolution of injected pure supercritical CO_2 or gaseous CO_2 may take thousands of years because of the absence of strong mixing (convective-diffusion dominated processes). Dissolving CO_2 in brine before injection significantly increases the security of geological sequestration. The mass transfer from CO_2 droplets into brine during cocurrent (CO_2−brine) horizontal pipe flow is studied mathematically to investigate the effectiveness of the proposed method. The dissolution rate of the CO_2 droplets is correlated to the variation of mean droplet diameter versus time, because the mass transfer causes shrinkage of the droplets. Empirical correlations based on Sherwood numbers were employed in the example for calculation of mass-transfer coefficients for droplets of CO_2 in the fluid flowing through a pipe.

1. INTRODUCTION

Greenhouse gas (GHG) emissions, particularly carbon dioxide (CO_2), represent a major environmental concern when talking about climate change.[1−4] These emissions are considered as the major contribution to global warming. Assessments reported by the Intergovernmental Panel on Climate Change (IPCC) emphasize that carbon capture and storage (CCS) can play an important role in minimizing the effects of climate change.[3] Geologic sequestration of CO_2 into deep saline aquifers represents a promising technique to mitigate the CO_2 concentration in the atmosphere.[1−5] The petroleum industry is moving toward integrated CO_2 capturing from power plants and injecting into underground formations, such as depleted oil and gas reservoirs and aquifers. Saline aquifers are considered as one of the promising options for CO_2 sequestration.[1,3] Nevertheless, significant uncertainties remain regarding the safety of long-term storage of CO_2 sequestration and the associated risks, such as leakage through high permeability zones in the aquifer, faults and fractures, which penetrate into the cap rock, poor cement job around the wellbores, abandoned wells, and open boundaries.[6−10] A semi-analytical approach proposed by Nordbotten et al.[6] presents an efficient prediction for leakage rates for the case of injection of supercritical CO_2 into a deep aquifer. However, it is limited by several important assumptions (e.g., ignoring mass transfer between phases and assuming constant values for density and viscosity).

Injection of CO_2 into the formations results in mobile CO_2, which can be in the form of gas or supercritical fluid. Because injected CO_2 is typically less dense than the resident fluids,[11−13] it may flow upward and leak to the ground because of gravity-driven flow (buoyancy effect).

Several studies have been conducted on determining CO_2 and brine properties (e.g., density and viscosity) as well as modeling diffusive-convective mechanisms in CO_2 sequestration.[9−17] Vilarrasa et al.[11] proposed an iterative method for calculating CO_2 density based on the solutions proposed by Nordbotten et al.[12] and Dentz and Tartakovsky[13] for the CO_2 bubbles in the aquifer, considering the CO_2 density as a nonlinear function of the formation and fluid properties.

Riaz et al.[15] presented a linear stability analysis of density-driven miscible flow in the context of CO_2 sequestration in saline aquifers. Their approach can explain the instability mechanisms of the long-wave cutoff and the critical time for the onset of convection in a semi-infinite domain.

After injection while employing the standard CO_2 sequestration technique, CO_2 dissolves slowly in the reservoir fluid and the time needed for the CO_2 to dissolve completely, by diffusion or natural convection, is typically on the order of 10^2−10^4 years, depending upon the reservoir conditions.[9−15] Hidalgo and Carrera[17] concluded that such time for the onset of convection will be in the order of months if dispersion is taken into account as a main transport mechanism for CO_2. Even for the latter case, the presence of mobile CO_2 underground for such a long period can cause huge difficulties to ensure the safety and public acceptance of the CCS technology.[1,9−15]

CO_2 leakage may cause health influences to humans, animals, and ecosystems at high concentrations. Long-lasting exposure to elevated CO_2 levels, above 20−30%, will result in death by suffocation.[18,19] For example, the rapid release of 0.24 megatons of CO_2 from Lake Nyos, Cameroon, led to the death of at least 1700 people and 4000 animals in 1986.[19]

Robust and efficient engineering methods are needed to be developed to accelerate the currently too slow rate of CO_2 dissolution sequestered into the sedimentary basins (e.g., saline aquifers), which in principle can be *ex situ* and/or *in situ*. The later allows for lowering the dissolution time to hundreds of years,[10]

Received: February 7, 2011
Revised: June 1, 2011
Published: June 06, 2011

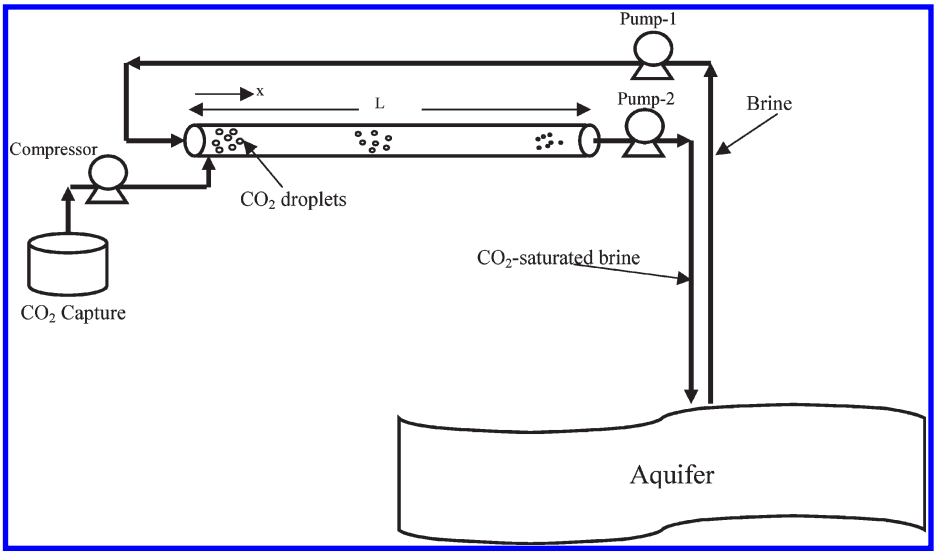

Figure 1. Schematic of *ex situ* dissolution of CO_2.

although the main weakness of this approach is the difficulty to ensure that injected brine efficiently dissolves CO_2. The *ex situ* dissolution aims to dissolve CO_2 into brine on the ground before injection.[10] Surface or *ex situ* dissolution could be achieved within a pipeline operating at the pressure of the target reservoir into which CO_2 is to be injected.[10]

The generation of CO_2 droplets sufficiently small to achieve rapid dissolution might rely on turbulent two-phase flow within the pipe. Such an approach can reduce the risks of CO_2 storage by the mean of reducing the time over which buoyant free-phase CO_2 is present underground. Also, it can simplify the risk assessment by reducing uncertainty of the long-term fate of injected CO_2 and expand the range of reservoirs that are acceptable for the storage purpose.[9,10]There are very high permeable formations that can be good candidates for the proposed method, for instance, an underground formation used for wastewater in southern Florida, where more than 2 gigatons of wastewater per year are injected 1 km down.[20]

In this paper, a new *ex situ* option that focuses on turbulent two-phase flow is introduced. Mass transfer from CO_2 droplets to saline water is studied mathematically to investigate the effectiveness of the proposed method. An analytical model is developed to predict the behavior of CO_2 droplets within the brine phase in a turbulent flow. More specifically, CO_2 liquid droplets in brine in a horizontal pipeline are considered here under a constant pressure in the system. The droplets are assumed to be spherical, and also the drop sizes are considered to be bigger than the inner turbulence scale (l) estimated according to $l \propto 5.3DRe_f^{-3/4}$, where Re_f is the Reynolds number for pipe flow and D is the pipe diameter.[21,22] Furthermore, the effects of the bulk liquid velocity, pipe length, and droplet and pipe diameters on dissolution of CO_2 liquid drops in a horizontal pipe are numerically investigated. The quantitative results are summarized for a case study at real scale to find out the variation of the droplet diameter for different ranges of droplet Reynolds numbers, which may lead to either diffusive or turbulent mass-transfer regimes. Results from this study indicate that it is technically feasible to dissolve most CO_2 on the ground before injection into the target formation.

2. MATHEMATICAL MODEL

A schematic view of the *ex situ* dissolution of CO_2 is shown in Figure 1. Compressed liquid-phase CO_2 from the capture source is injected into the horizontal pipeline where the brine (produced from the target aquifer) is flowing. The flow turbulence within the pipeline breaks CO_2 into the droplets that dissolve in the brine while being carried along the pipeline flow. Finally, CO_2-saturated brine is reinjected to the aquifer.

The efficiency of the dissolution process (η) can be defined as

$$\eta = \frac{V_p(inlet) - V_p(outlet)}{V_p(inlet)} = 1 - \left(\frac{d_p(t_{max})}{d_p(t_0)}\right)^3 \quad (1)$$

Here, V_p(inlet) and V_p(outlet) are the volumes of droplets for the inlet and outlet points of the pipeline, respectively. $d_p(t_{max})$ is the droplet diameter at output (final) conditions, and $d_p(t_0)$ is the droplet diameter at input (initial) conditions. $\eta = 1$ means that the injected CO_2 is completely dissolved in the brine, and the size of CO_2 droplets approaches zero when they reach the end of the pipeline at $t = t_{max}$.

A mathematical model was developed for mass transfer from a single droplet of CO_2 to the surrounding flow to investigate the different aspects of CO_2 dissolution in a pipeline and to find the controlling factors affecting the process efficiency.

The rate of mass transfer from a single droplet can be expressed as

$$-\frac{dm}{dt} = kA\Delta C \quad (2)$$

where $-dm/dt$ is the rate of mass transfer from the droplet into surrounding liquid, k is the mass-transfer coefficient, A is the droplet surface area, and ΔC is the difference in concentration, which drives the dissolution process. Assuming that flow is isothermal and the droplet is composed of pure CO_2, the concentration gradient can be written as follows:

$$\Delta C = C_s - C_\infty \quad (3)$$

where C_s and C_∞ are the CO_2 concentrations at the droplet−liquid interface and in the brine, respectively.

It is assumed that the volume of brine is very large compared to a droplet volume (which is reasonable in most real cases and will be discussed later). It is also assumed that there is no CO_2 initially dissolved in the brine. Therefore, the CO_2 concentration in the bulk liquid phase, C_∞, would be zero, and then eq 2 is expressed as

$$-\frac{dm}{dt} = kAC_s \quad (4)$$

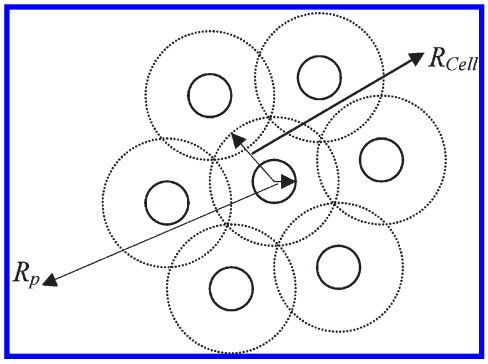

Figure 2. CO_2 drop in a cell of neighbors.

It should be noted here that the above assumptions are valid only if there is one single droplet surrounded by a large volume of the liquid continuum; otherwise, it is inevitable to consider the interaction between the droplets and the surrounding liquid. This interaction effect on the average concentration in the bulk brine phase will be explained later.

The continuity equation for the liquid leaving the droplet is

$$\frac{dm}{dt} = \frac{\pi {d_p}^2}{2}\rho_p \frac{d(d_p)}{dt} + \frac{\pi {d_p}^3}{6}\frac{d\rho_p}{dt} \tag{5}$$

where d_p and ρ_p are the droplet (or particle) diameter and the density, respectively.

It is assumed that the pipeline pressure drop because of the wall friction is small (~0.5 bar based on the estimation performed using Appendix A). Therefore, a constant density for a CO_2 droplet flowing through the pipe is expected, and the equation of mass conservation for a droplet can be written as

$$\frac{dm}{dt} = \frac{\pi d_p^2}{2}\rho_p \frac{d(d_p)}{dt} \tag{6}$$

By substitution of eq 6 into eq 2, we obtain the following form of the governing equation for mass transfer from a single liquid drop:

$$\frac{d(d_p)}{dt} = \frac{2k(C_s - C_\infty)}{\rho_p} \tag{7}$$

where C_∞ is a concentration of CO_2 in the ambient liquid.

In general, because of a small but finite CO_2 holdup, the presence of multiple droplets (particles) and their impacts needs to be taken into account while these droplets dissolve in the brine phase simultaneously. In this study, a basic approach[23,24] is proposed as the droplet is placed within the center of a liquid cell radius (R_{cell}) on the cell boundary (see Figure 2).

$$\frac{\partial C}{\partial r} = 0 \quad at\ r = R_{cell} \tag{8}$$

The influence of surrounding droplets is taken into consideration by a simple assumption that the concentration of CO_2 in the ambient liquid is equivalent to an average value $C_\infty(t)$ at any time t. Because the distance between the droplets is much larger than that of the diffusion layer, the CO_2 concentration inside the cell will remain unchanged during the mass-transfer period. Consequently, the relationship between the CO_2 concentration in the liquid phase and that in the droplet for two different times could be expressed as the following equation (mass conservation):

$$\rho_{p,0}V_{p,0} + C_{\infty,0}V_{L,0} = \rho_p(t)V_p(t) + C_\infty(t)V_L(t) \tag{9}$$

where V_p and V_L are the droplet volume and ambient liquid phase, respectively. Also, subscript 0 refers to initial conditions.

On the other hand, we can write the following basic formula to relate droplet volume (V_p) to the ambient liquid phase (V_L):

$$V_{cell} = V_p + V_L \tag{10}$$

where V_{cell} is the total volume of the liquid cell.

On the basis of the previously made assumptions, the initial CO_2 concentration, $C_{\infty,0}$, is zero and droplet density, ρ_p, is constant along the pipe length. Additionally, in a real pipeline flow, the change in the cell volume, $V_L = (1 - \phi)V_{cell}$, is small compared to the change in the void fraction volume. Applying this assumption, it can be concluded that

$$V_{L,0} \approx V_L(t) \approx cte \tag{11}$$

$$V_{cell,0} \approx V_{cell}(t) \approx cte \tag{12}$$

where ϕ is the holdup (void fraction) of droplets.

On the basis of the hypothesis expressed in eqs 10−12 and also the assumption of constant density for the CO_2 phase, using the volume expression for the droplet, the average CO_2 concentration for the ambient phase can be derived from eq 9 as follows:

$$C_\infty(t) = \frac{\rho_p \phi_0}{1 - \phi_0}\left[1 - \left(\frac{d_p}{d_{p,0}}\right)^3\right] \tag{13}$$

Here, ϕ_0 and $d_{p,0}$ are the initial void fraction and the initial droplet diameter of the CO_2 phase, respectively.

Then, we incorporate eq 13 into eq 7, and the following relationship can be obtained:

$$\frac{d(d_p)}{dt} = \frac{2kC_s}{\rho_p} - \frac{2k\phi_0}{1 - \phi_0}\left[1 - \left(\frac{d_p}{d_{p,0}}\right)^3\right] \tag{14}$$

In this equation, k is a function of time, because it depends upon the droplet size and should be calculated at any instant time.

3. REQUIRED INPUT DATA FOR THE MASS-TRANSFER EQUATIONS

The following section provides necessary correlations for the mass-transfer coefficient, CO_2 solubility in brine, and initial size of CO_2 droplets, which are the main variables for our calculations.

3.1. Sherwood Number Correlations. The study of convective mass transfer from a liquid droplet (or/and a bubble) to an ambient fluid was first conducted by Levich.[21] Also, Clift et al.[22] have conducted numerous studies regarding the mass transfer from/to droplets. They reported various conditions of moving droplets at different values of the relevant dimensionless numbers, such as Schmidt number (Sc) and Reynolds number (Re_p).

Here, the Reynolds number is $Re_p = Ud_p/\nu$, and the Schmidt number is $Sc = \nu/D_{CO_2-brine}$, where U is the brine velocity, d_p is the CO_2 droplet diameter, ν is the kinematic viscosity, and $D_{CO_2-brine}$ is the diffusion coefficient of CO_2 in brine (refer to Appendix B for the calculation of the diffusivity coefficient).

The mass-transfer coefficient is crucial for the drop size change and the evolution of the droplet size distribution. The instantaneous value of k in eq 14 may be estimated by appropriate empirical correlations for Sh, defined as $kd_p/D_{CO_2-brine}$.

Turbulent-flow mass-transfer coefficients for drops flowing cocurrently with liquids in a pipeline were determined using transient response experiments by Kress and Keyes.[25] On the basis of their study, for high pipe Reynolds numbers that turbulent inertial forces dominate over the gravitational forces,

horizontal and vertical flow mass-transfer coefficients are equal to

$$Sh = 0.34\left(\frac{d_p}{D}\right)^2 Re_f^{0.94} Sc^{0.5} \quad (15)$$

where Re_f is given based on brine properties and pipe diameter as UD/ν, where ν is the kinematic viscosity of brine, μ/ρ, in the definition of Re_f, and D is the pipe diameter.

There is also a well-known correlation for the mass-transfer coefficient based on experimental results proposed by Ranz and Marshal.[26]

$$Sh = 2 + 0.6 Re_p^{1/2} Sc^{1/3} \quad (16)$$

Scott and Hayduk[27] dissolved carbon dioxide and helium into water, ethanol, and ethylene glycol in horizontal pipeline flow, where turbulent bubbly flow had been established. Their results were correlated by the equation as expressed below

$$Sh = 0.0087955 U d_p^2 \phi^{-0.926} \sigma^{0.51} \mu_{brine}^{0.08} D_{CO_2-brine}^{-0.61} / D^{1.88} \quad (17)$$

where ϕ is the volumetric fraction of CO_2 droplets, σ is the surface tension, and μ_{brine} is the viscosity of the brine phase (see Appendix C for the calculation of the brine viscosity). Units of all variables are in the SI system for the above correlation.

3.2. Solubility of Liquid CO_2 Droplet in Brine. Liquid CO_2 and brine are very dissimilar in their physical properties. Liquid CO_2 is a nonpolar substance, while brine has a strong polarity. Therefore, the solubility of liquid CO_2 in brine is much larger than that of brine in liquid CO_2. The CO_2−brine solubilities have been studied extensively in the literature.[28−37] In this section, a brief review of some of the studies is presented. Span and Wagner[28] reviewed the available data on thermodynamic properties of the CO_2−water mixture and obtained a new correlation in the term of the Helmholtz free energy, which represents the experimental data precisely. Additionally, a non-iterative approach was proposed by Spycher and Pruess[29] to compute mutual solubilities for solutions up to 6 mol/kg NaCl and 4 mol/kg $CaCl_2$. This was accomplished by combining the solubility correlation by Spycher et al.[30] with the activity coefficient formulation by Rumpf et al.[31], and Duan and Sun.[32]

The solubility of CO_2 (C_S) may be expressed as follows:[35]

$$C_S = \frac{x_{CO_2}\rho_{brine}}{(1 - x_{CO_2})M_{w,brine}}\left(\frac{44\ kg}{1\ kmol}\right) \quad (18)$$

where C_S is the solubility of CO_2 in the liquid phase, x_{CO_2} is the solubility of CO_2 in a mole fraction, and $M_{w,brine}$ is the molecular weight of brine. The solubility of CO_2 in a mole fraction is expressed by the modified Henry's law.

$$x_{CO_2} = \frac{f_{CO_2}}{K_H} \quad \text{for pure water} \quad (19)$$

$$x_{CO_2} = \left(\frac{f_{CO_2}}{K_H}\right) e^{\alpha S} \quad \text{for brine} \quad (20)$$

S is the salinity of brine, which is defined as the total dissolved salts in the solution in mass percent, and α represents the salting-out coefficient in eq 20.

In the calculation, Henry's law constant (K_H) and the salting-out coefficient by Teng and Yamasaki[36] were adopted. CO_2 fugacity is determined from the Peng−Robinson (PR) equation of state (EOS) (see Appendix D for more details).

Furthermore, according to the research performed by Bando et al.,[37] the relationship in solubilities between brine and pure water could be expressed as

$$C_S \text{ (in brine)} = 0.85 C_S \text{ (in pure water)} \quad (21)$$

The above expression leads to acceptable data for CO_2 solubility in some real cases at moderate temperatures (20−100 °C) and pressures (0−80 bar). Also, the salinity for this correlation should be in the range of 0.5−1.4 mol/kg.

3.3. Correlation for Droplet Size. In our case, the initial size of the droplet is one of the required parameters to obtain the droplet size and concentration of the ambient phase along the pipe length at various times to solve eq 14.

For the bubbly flow regime, the Weber number ($We = \rho_{brine} U^2 d_p/\sigma$) decides the competitive effects of inertia and surface tension forces and, thus, the likelihood of a drop to experience further breakup.[21,22] Hibiki et al.[38] experimentally determined the critical value for the dimensionless Weber number and proposed the following expression for the maximum stable droplet size ($d_{p,max}$) during the turbulent drop−liquid system:

$$d_{p,max} = 4\sqrt{\frac{\sigma}{g\Delta\rho}} \quad (22)$$

where g and $\Delta\rho$ are the gravitational acceleration and the density difference, respectively.

Another work regarding the droplet size is the research conducted by Angeli and Hewitt,[39] who investigated the influences of important aspects of two-phase flow on the drop size distribution, where the droplet volume fraction changes from 3 to 9%. This study was performed on different fluid pairs, flow regimes, and pipe properties. The experimental and theoretical results on the maximum diameter were represented satisfactorily by the following equation, which considers the continuous phase velocity and the nature of the continuous phase and pipe material through the friction factor, f:

$$\left(\frac{d_{p,max}\rho_{brine}U^2}{\sigma}\right)\left(\frac{f d_{p,max}}{4D}\right)^{2/3} = 0.369 \quad (23)$$

At low dispersed phase viscosities, eq 23 gives results with high accuracy.

In the literature, several analytical formulations have also been proposed to estimate the minimum droplet size in two-phase, two-component flow.[21,22]

The minimum diameter of a drop ($d_{p,min}$), which is stable in a turbulent dispersion with a tangentially immobile interface, is expressed as[40]

$$d_{p,min} = \left(\frac{\sigma^{1.38} C_{L-V}^{0.46}}{0.0272 \mu_{brine}\rho_{brine}^{0.84}\varepsilon_0^{0.89}}\right)^{0.321} \quad (24)$$

where C_{L-V} is the London−van der Waals constant and is assumed to be 10^{-28} J mol/kg and ε_0 is the rate of energy dissipation for pipe flow because of turbulence, defined as $f(U^3/2D)$.

Now, we can have a range of initial drop sizes for the current study. Therefore, it is possible to investigate the impact of the initial droplet size on the concentration distribution of CO_2 and change the rate of the diameter during the dissolution process by considering three different sizes for the initial diameter.

4. FURTHER TECHNICAL ISSUES

In this section, technical issues on the efficiency of the proposed method that challenge the long-term success of any large-scale CO_2 sequestration project are discussed. Also, a brief explanation is presented here about other issues, such as geological and geomechanics issues, which are beyond the purpose of this paper.

4.1. Dissolution Efficiency. One of the important parameters in evaluation of the introduced methodology is the dissolution efficiency (η), which is defined here as the ratio of the mass (volume) of dissolved CO_2 because of *ex situ* dissolution to the initial mass of injected CO_2 (see eq 1).

In standard sequestration methods that involve bulk injection of CO_2 without brine, 6.5% CO_2 is dissolved during the 20 years of CO_2 injection and only an additional 1.5% dissolves over 300 years according to numerical simulations reported in the literature.[10] However, with brine injection at a rate of 1 megaton/year flowing through the pipeline, over 95% CO_2 is dissolved within about 300 s because of the convective-turbulence mechanism (refer to the example presented in this study) .

4.2. Brine Flow Rate Required for *ex Situ* Dissolution. The brine flow rate, produced from the saline aquifer, depends upon the CO_2 flow rate supplied from the capture facility and also thermodynamic conditions of the pipeline. If it is assumed to provide enough pipe length for complete dissolution, then the equilibrium mass percentage of CO_2 in the solution will be usually in the range of 4−7%, depending upon the temperature and pressure.[30,41−43] Under typical storage conditions (pressure, ∼100−150 bar; temperature, ∼50−75 °C; and salinity, 0−10% of solid by weight), the concentration of the dissolved CO_2 is 5 wt %.[30,41−43] Hence, the ratio of brine mass flow to CO_2 mass flow is 20 for the *ex situ* dissolution process. For instance, the required brine flow rate for annual disposal of 0.05 megaton of CO_2 is 1 megaton/year (see the case study presented in this paper).

4.3. Economics. There is no doubt that the *ex situ* dissolution process can accelerate the dissolution significantly, but the vital problem is at what cost? A rough estimate of additional costs for the required equipment, well, and electrical energy is made here for the introduced scheme. It is intended here to compare the extra cost for the *ex situ* dissolution to the total cost needed for a CCS plant. The main part of costs for the *ex situ* approach originates from the cost of energy required to produce brine and the capital costs of the pumps and any extra wells. The present cost for the required drilling and well completion is on the order of $10 million.[3,4] The capital cost of the required pumps and related controls would be around $50 000, which is not significant compared to the cost associated with wells. Assuming a flow rate of 1 megaton/year for injection into the aquifer, then the required electrical power would be around 85 kW, considering the pump with an efficiency of 75%. Because the electricity cost for North American industrial companies is on the range of $80−100/MWh,[3,4] the annual operating cost for injection/production pumps would approach $80 000. Moreover, the total capital cost for a full CCS project is estimated to be around $450 million for each 1 megaton/year of CO_2 sequestered in the saline aquifer.[3,4] In this case, the capital cost of the *ex situ* dissolution process is estimated to be ∼2% of the capital cost of the full CCS plant.

Using the rough cost estimations above, the total cost to accelerate the dissolution of the injected CO_2 over a 300 year period will be ∼$0.09 a ton of CO_2, which is lower than 0.2% of the typical costs of lowering CO_2 emissions employing a CCS technology.

4.4. Geochemistry and Acidification. Geochemical reactions play important roles when evaluating effects of CO_2 storage long term. The major geochemical reaction identified in some formations is the precipitation of Dawsonite as an aluminum carbonate mineral that can make up to 17% of the reservoir.[44−46] Moreover, geochemical interactions between the aqueous solution of CO_2 and rock-forming minerals are very possible to occur, involving both dissolution and precipitation.[45−47] Geochemistry probably influences the chemical and physical properties of the wells, the formation, and its surroundings because of the potential corrosive character of CO_2.[44,48] Therefore, it may increase the environmental and financial risks of the CO_2 sequestration projects in deep geological formations.

When CO_2 is dissolved in the brine phase, carbonic acid is created as follows:

$$CO_2 + H_2O \rightarrow H_2CO_3 \qquad (25)$$

Carbonic acid is corrosive to piping, valves, seals, and O-rings; therefore, it is necessary to consider a secure design for surface equipment and injection wells. The additional expense to corrosion-resistant metallurgy was not included in the capital costs. It would increase the injection well costs approximately 1.8 times.[3,4] Precipitation of minerals can happen at high percentages of salinity because of the introduction of new ions and the effect of carbonic acid on the pH of the brine phase flowing through the pipeline.[45,47] The injectivity might be affected by mineral participation in the pipe, wellbore, or near-wellbore region of formation.

The carbonated water (carbonic acid) needs special handling to prevent the formation of hydrate in the pipeline and special materials of construction that must be resistant to the corrosive action of the carbonated stream. Hence, the stream containing water and CO_2 cannot be transported through carbon steel pipes, but corrosion-resistant metallurgy could be added in carbon steel pipes to lower corrosion.[49] It is recommended that corrosion-preventive actions are assessed and performed. The efficient actions can include selection of appropriate operating conditions and corrosion inhibitor materials. One of the proper metals for this application is 304/316L stainless steel, which was verified to be the best for corrosion resistance.[50]

It should also be noted here that the formation of carbonic acid (carbonated water) makes CO_2 much less buoyant in the subsurface, which can reduce the leakage risk.

An accurate prediction of reaction rates between rock, CO_2, and brine is an important issue, if CO_2 sequestration within deep aquifers is to gain industrial-scale satisfaction with government regulations.

4.5. Geology and Geomechanics. Cap rock fracturing during injection is an issue for CCS technologies.[51−53] Thus, the geomechanical stability and cap rock integrity should be taken into account in research studies as well as implementation of CO_2 sequestration projects.[51−53] However, the brine production wells prevent buildup of pressure in the aquifer for the *ex situ* dissolution scheme. This leads to the reduction in the risk of fracturing the storage geological formation or the seal during injection. It also significantly lowers the risk that injection rates will be constrained by rising formation pressure.

It should be noted here that 180 bar estimated for our case study is not an issue for this particular problem, because fracture pressure is typically 1.5−3 times higher than hydrostatic

pressure.[10,54] However, bottom-hole pressure (BHP) will usually be higher during the injection in practice, which will limit the injection flow rate.[51−53] This would imply the perforation of several injection wells, instead of a single well for injecting CO_2−brine solution into the saline aquifer.

5. EXAMPLE AT A REALISTIC SCALE

Considering an *ex situ* dissolution process for CO_2 sequestration, the brine solution is produced from the aquifer and then flows with high velocity in a horizontal pipe. Simultaneously, the CO_2 stream is injected from the storage to the pipeline. The process is isothermal with a temperature of 20 °C, and also the pressure of the input brine phase is 70 bar, which remains constant along the pipe.

Because the temperature in the real formation (e.g., Mt. Simon formation) varies from 25 to 35 °C,[43] it is essential to keep the pressure above 65 bar to maintain CO_2 in liquid or supercritical phase. The reason is that if just a single liquid phase of the mixture is injected into the formation, saturation fronts, mobility contrasts, and fingering would be eliminated. In addition, the density difference between CO_2-laden brine and native brine is small under these thermodynamic conditions, leading to reduction in gravity-driven segregation. The above explanation supports the selected pressure (70 bar) along the horizontal pipeline in this example.

Table 1. Known Parameters for the Modeling Problem

parameters	value
pipe diameter, D (m)	0.15
pipe roughness, Ro (m)	45×10^{-6}
surface tension, σ (mN/m)	33
brine density, ρ_{brine} (kg/m^3)	1029
CO_2 density, ρ_{CO_2} (kg/m^3)	810
brine viscosity, μ_{brine} (mPa s)	1.08
CO_2 viscosity, μ_{CO_2} (mPa s)	0.07341
salinity, S (%)	10

The characteristics of the process, such as the pipe diameter, brine density, and viscosity, and CO_2 physical properties are summarized in Table 1 below. The physical properties for CO_2 and brine are obtained at T = 20 °C and P = 70 bar, using appropriate empirical correlations/values.[32,33,55] In the following example, we carried out a number of computations to illustrate the CO_2 droplet dissolution in a turbulent flow. A summary of numerical modeling runs conducted during this study is provided in Table 2. In this table, the runs are organized for different process variables, such as the droplet properties (i.e., diameter and droplet holdup), pipeline properties (length and liquid flow rate), and also correlations of the Sherwood number. Relatively wide ranges of vital parameters (see Table 2) contributing in the mass-transfer process are considered for a fairly comprehensive sensitivity analysis to characterize the behavior of CO_2 drops. An important aspect in the *ex situ* dissolution process is to sparge enough amount of CO_2 into the brine phase. On the basis of the *PVT* studies, the solubility of CO_2 in brine under *in situ* aquifer conditions is between 4 and 7 wt % for a depth greater than 650 m, depending upon temperature and pressure conditions.[30,41−43]

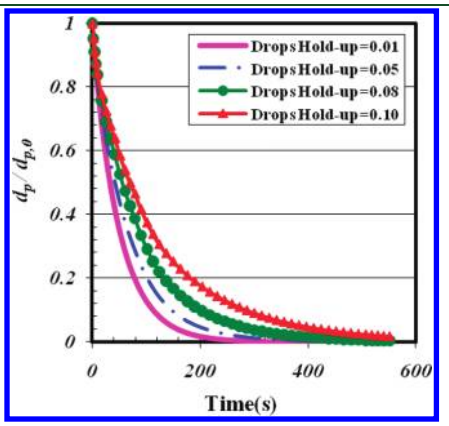

Figure 3. Ratio of the droplet diameter to the initial diameter versus time for the horizontal pipe with different drop volume fractions.

Table 2. Process Conditions for All of the Runs Conducted in Mathematical Modeling

		CO_2 droplet		pipe	
modeling variable	case number	droplet diameter (mm)	CO_2 holdup (%)	pipe length (km)	brine flow rate ($\times 10^3$, m^3/s)
droplet size	1	2.0×10^{-3}	5.0	1.0	32.0
	2	2.0	5.0	1.0	32.0
	3	20.0	5.0	1.0	32.0
CO_2 holdup	4	2.0	1.0	1.0	32.0
	5	2.0	5.0	1.0	32.0
	6	2.0	10.0	1.0	32.0
pipe length	7	2.0	5.0	0.1	32.0
	8	2.0	5.0	1.0	32.0
	9	2.0	5.0	3.0	32.0
brine flow rate	10	2.0	5.0	1.0	8.0
	11	2.0	5.0	1.0	16.0
	12	2.0	5.0	1.0	32.0
Sherwood number	13	2.0	5.0	1.0	32.0 (eq 15)
	14	2.0	5.0	1.0	32.0 (eq 16)
	15	2.0	5.0	1.0	32.0 (eq 17)
	16	2.0	5.0	1.0	diffusive dissolution (Sh = 2)

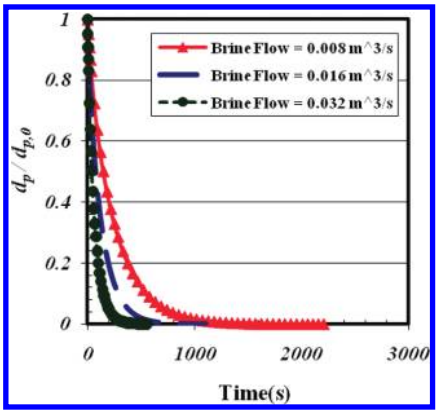

Figure 4. Effect of the brine flow rate on dissolution behavior.

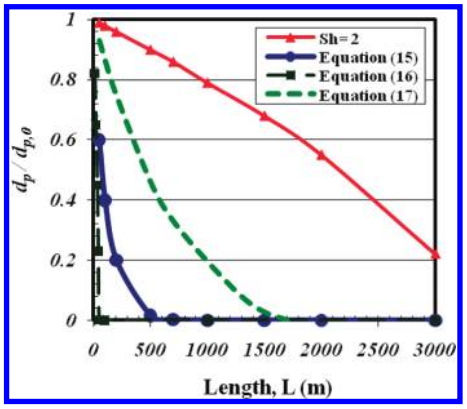

Figure 5. Profile of shrinkage of the liquid CO_2 droplet in brine along the pipe length at different flow regimes.

Therefore, 5% is selected for the volume fraction of CO_2 in most cases (Table 2). For the purpose of this sensitivity analysis, drop size values are selected between maximum and minimum stable sizes (eqs 22−24).

On the basis of the analytical solution, the influences of process variables on the ratio of the final droplet size to the initial droplet size as well as the magnitude of the mass-transfer rate are studied. Here, we present some modeling results.

Figure 3 depicts variations of droplet size (a good indicator of the dissolution rate) calculated from eq 14 as a function of the droplet holdup while the droplets move along the pipe. As can be found from the expression $\phi_0\rho_p V_{cell}$, the droplet volume fraction causes an increase in the average concentration of CO_2 dissolved in the ambient brine phase, reducing the concentration difference on the droplet boundary and, consequently, lowering the rate of mass transfer. Modeling outputs based on eq 14 clearly demonstrate the impact of CO_2 holdup.

Figure 4 shows the droplet size change at brine flow rates between 0.25 megaton/year (0.008 m^3/s) and 1 megaton/year (0.032 m^3/s). Rates of reduction in diameter were different because a greater brine flow rate causes more turbulence and, thus, a higher mass-transfer rate; therefore, the shrinkage rate in this theoretical study is the highest for 0.032 m^3/s and the lowest for 0.008 m^3/s.

In Figure 5, the dissolution behavior of CO_2 droplets is shown as the pipe becomes longer. When the initial diameter of the CO_2 droplet is 2 mm, dissolution is completed in the length of 500 and

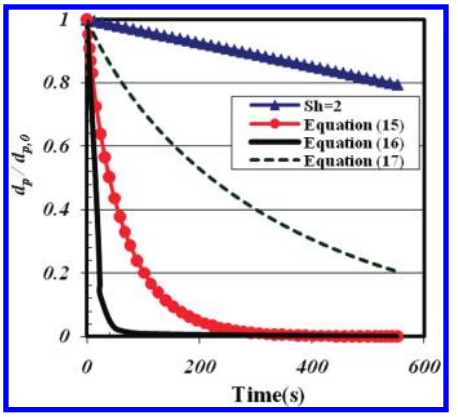

Figure 6. $d_p/d_{p,0}$ versus time for different Sherwood correlations.

1700 m based on eqs 15 and 17, respectively, while according to eq 16, complete dissolution occurs at almost 50 m. Equation 16 predicts higher mass-transfer rates than eqs 15 and 17. For laminar dissolution, in which molecular diffusion is predominant, dissolution is not completed even at 3000 m of pipe length. This case is presented as a benchmark for the slowest possible rate, because in the cases presented here, all flow regimes are turbulent and dissolution rates are higher than the rate of laminar dissolution.

The effect of the type of Sherwood correlation selected for this investigation is shown in Figure 6. Again, the figure conveys the message that an exact value for the mass-transfer coefficient is necessary to predict with high accuracy at different times. Regardless of the type of Sherwood correlation employed in the calculation, we have almost full dissolution in the pipeline if the length is 1650 m and the brine flow rate and pipe diameter are 1 megaton/year and 15 cm, respectively.

The changes of the dimensionless diameter ($d_p/d_{p,0}$) of a single CO_2 droplet to t = 600 s for different initial droplet sizes from 20 to 0.002 mm are shown in panels a−c of Figure 7. Note that the dissolution behavior differs substantially depending upon which correlation of the Sherwood number is used in the calculation. For example, eq 15 does not exhibit any difference between the values of the dimensionless diameter for the droplets with various initial sizes. For this issue, we presented the results for eqs 15 in Figure 7a, while the results for eq 16 and the laminar dissolution regime (Sh = 2) are given in panels b and c of Figure 7, respectively. Because the mass-transfer rate from eq 16 is very high, the droplets decrease in size significantly, even if the drops are exposed to the brine phase for a short time only. Droplets smaller than 2 mm are completely dissolved under turbulent flow within 300 s, according to Figure 7. Another conclusion from Figure 7c is that the mass-transfer rate is low in laminar dissolution such that droplet size remains almost constant during the dissolution process when the initial droplet size is large enough (i.e., >0.02 m). In this situation, probably the droplet size at the exit is not much different from the initial value. Because the smaller the droplet size, the stronger its tendency to dissolve as a result of a higher specific area, the most effective approach to liquid CO_2 introduction is in as finely divided droplets as possible (high turbulent shear conditions at the input nozzle). On the other hand, at some point of flow, droplets reduced to the scales comparable to the inner turbulent scale ($I \sim 0.70$ mm), where the laminar (diffusive) regime is dominating even in overall turbulent flow.

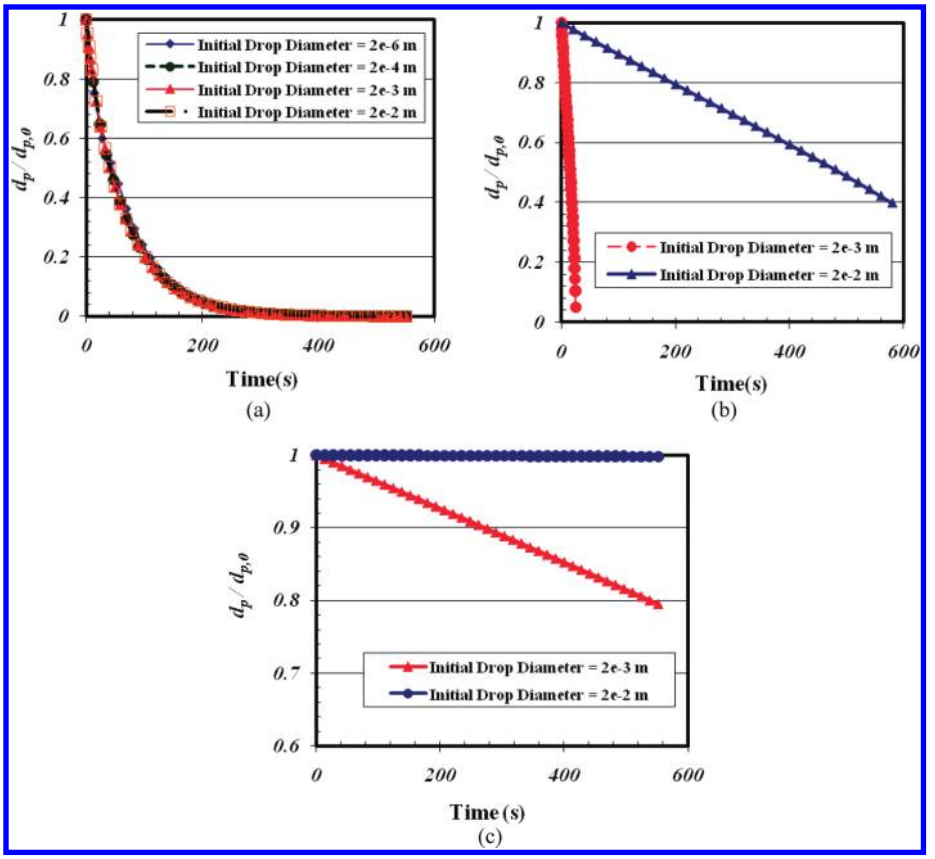

Figure 7. Dependencies of droplet size change in time at various initial drop sizes for different correlations of the Sherwood number: (a) eq 15, (b) eq 16, and (c) laminar flow ($Sh = 2$).

Thus, the model developed enables us to explore the CO_2 droplet behavior if suitable empirical equations for the mass-transfer coefficient are known and then applied to the governing equation of mass transfer from liquid droplets to the ambient phase. Dubious results from uncertain Sherwood numbers impede reliable assessment of the drop behavior under isothermal and isobaric conditions, and the main problem for confident analysis is the absence of acceptable data for liquid CO_2 droplet dissolution in turbulent and laminar flow.

CONCLUSION

Dissolution of CO_2 droplets during cocurrent CO_2−brine turbulent flow through a horizontal pipeline has been investigated at isothermal conditions. This study introduces a new methodology for acceleration of CO_2 dissolution that could be beneficial in providing a far greater CO_2 storage security as well as capable of being used along with deep disposal of saline water, such as co-produced water from oil and gas wells.

The main results of this study can be summarized as follows: (1) A physical model for mass transfer from CO_2 droplets into brine during cocurrent (CO_2−brine) horizontal pipe flow has been developed. The mass-transfer coefficient was estimated using different empirical correlations for the Sherwood number, and corresponding dissolution rates have been calculated for a variety of conditions. (2) To achieve maximum dissolution without free CO_2, an equation for engineering applications is proposed on the basis of the mass-transfer approach in terms of initial droplet size, temperature, pressure, and pipe length. (3) It was found that initial droplet size and CO_2 holdup are the dominant parameters governing the dissolution rate. A smaller initial drop size leads to more rapid dissolution. CO_2 holdup, even as small as 1−2%, reduces the mass-transfer rate and, thus, the droplet shrinkage rate. (4) The dissolution rate increases with the increase of brine flow velocity. Moreover, the total amount of dissolved CO_2 in brine increases up to the saturation point as the pipeline becomes longer. The CO_2 dissolution rate within the turbulent regime is a function of the flow velocity ($dm/dt \sim Re^n$), where n ranges from 0.5 to 1.0. The n value depends upon the type of empirical Sherwood correlations implemented in the numerical model. (5) The fairly large difference between numerical results obtained for various correlations of the Sherwood number indicates the necessity for experimental investigations of the droplet flow in a pipeline to predict CO_2 dissolution behavior in brine with confidence. However, the most important result is even at a worst case scenario ($Sh = 2$); it is possible to dissolve a substantial amount of CO_2 before injection. All other cases will produce higher dissolution rates. (6) Further theoretical work, economic analysis, and experiments are needed to test whether this method can be applied on a large scale. While no single approach is likely to solve the entire CO_2 sequestration problem, this dissolution technique for sequestering fossil-fuel carbon could contribute significantly to the issue of global CO_2 mitigation.

APPENDICES

Appendix A: Friction Factor for Turbulent Pipe Flow. The general behavior of turbulent pipe flow in the presence of surface

dx.doi.org/10.1021/ef200199r |*Energy Fuels* 2011, 25, 3323–3333

roughness is well-understood. In turbulent flow, the friction factor (f) depends upon the Reynolds number (Re_f) and the relative roughness of the pipe, Ro/D. The three promising equations for the friction factor have appeared as follows:

(1) Swamee and Jain:[56] They obtained the correlation covering the range of Re_f from 5000 to 10^7 and the values of Ro/D between 0.000 04 and 0.05 as

$$f = \frac{0.25}{\left[log\left(\frac{Ro}{D} + \frac{5.74}{Re_f^{0.9}}\right)\right]^2} \quad (A1)$$

(2) Churchill:[57] The researcher claimed that the empirical equation is valid for all Re_f and Ro/D and has the following form:

$$f = \left(\left(\frac{8}{Re_f}\right)^{12} + (a+b)^{-3/2}\right)^{1/12} \quad (A2)$$

$$\text{where } a = \left[-2\, log\left(\frac{(Ro/D)}{3.7} + \left(\frac{7}{Re_f}\right)^{0.9}\right)\right]^{16} \text{ and } b = \left(\frac{37530}{Re_f}\right)^{16}$$

(3) Chen:[58] He also suggested a correlation for the friction factor that holds all of the ranges of Re_f and Ro/D.

$$\frac{1}{\sqrt{f}} = -2\, log\left[\frac{Ro}{3.7065D} - \frac{5.0452}{Re_f} log\left(\frac{1}{2.8257}\left(\frac{Ro}{D}\right)^{1.1098} + \frac{5.8506}{Re_f^{0.8981}}\right)\right] \quad (A3)$$

Appendix B: Molecular Diffusion Coefficient. A number of useful empirical equations are being commonly used to calculate the diffusion coefficients in water. For example, Wilke and Chang[59] have proposed a correlation to evaluate the diffusion coefficient of CO_2 in water at high pressures. The binary diffusion coefficient is given by

$$D_{CO_2-W} = 7.4 \times 10^{-8} \frac{(\beta M_{w,W})^{0.5} T}{\mu_W (V_{CO_2}^{bp})^{0.6}} \quad (B1)$$

where the unit of the diffusion coefficient of CO_2 in water (D_{CO_2-W}) in the above formula is in cm^2/s, β is an association parameter equal to 2.26 for water, $M_{w,W}$ is the molecular weight of water, T is the temperature in K, μ_W is the viscosity of water in cP, and $V_{CO_2}^{bp}$ is the molar volume of CO_2 at the normal boiling point in cm^3/gmol. The value of $V_{CO_2}^{bp}$ is 86.04 cm^3/gmol, according to the literature.[33,55]

When the diffusion coefficient of CO_2 into water is available, the diffusion coefficient of CO_2 into brine can be determined at a constant temperature and pressure according to the following equation:[60,61]

$$log\left(\frac{D_{CO_2-W}}{D_{CO_2-brine}}\right) = 0.87\, log\left(\frac{\mu_{brine}}{\mu_W}\right) \quad (B2)$$

Appendix C: Density and Viscosity of Brine. In sedimentary basins, physical properties of formation waters usually change by more than 25% for density and by 1 order of magnitude for viscosity, relative to freshwater at standard conditions, as functions of salinity, temperature, and pressure.[16] Density and viscosity increase with increasing salinity and pressure, but increasing temperature leads to a reduction in density and viscosity magnitudes.[16]

In reviewing aqueous-phase density, we noted that there is a reasonable estimate for the density of brine solutions in the study conducted by Sayegh and Najman[62] as follows:

$$\rho_{brine} = \frac{\rho_W}{M_{w,W}} M_{w,brine} \quad (C1)$$

where $M_{w,brine} = (1051.2/(58.4 - 0.404S))$ was suggested by Enric and Klare[28] for brine molecular weight ($M_{w,brine}$) in eq C1.

Additionally, Enric and Klare[63] employed several data sources for the viscosity of brine solutions, one tabular and one graphical, to develop the following correlation, which relates brine viscosity to that of pure water for the temperature range of 293−373 K under the assumption that the effects of pressure are ignored:

$$\mu_{brine} = \mu_W[1 + (1.892 \times 10^{-2})S + (1.215 \times 10^{-4})S^2 + (1.941 \times 10^{-5})S^3] \quad (C2)$$

in which μ is in cP (mPa s).

Appendix D: Fugacity and Henry's Constant. On the basis of PR EOS, Duan et al.[32,33] proposed a non-iterative EOS to calculate the CO_2 fugacity as a function of the temperature and pressure

$$f_{CO_2} = c_1 p + [c_2 + c_3 T]p^2 + [c_4 + c_5 T]p^3 + [c_6 + c_7 T] + [c_8/T + c_9 T^2]p \quad (D1)$$

where T is in K and p is in bar (Table D1).

The parameters c_1, c_2, c_3, ..., c_8, and c_9 were fitted to f_{CO_2} calculated from the EOS by Duan et al.[32,33] at the $T-P$ range where CO_2 droplets are in liquid state.

Teng and Yamasaki[36] determined the dependence of Henry's law constant and the salting-out coefficient on the temperature and pressure as follows:

$$K_H = a + bp + cp^2 \quad (D2)$$

with

$$a = 5.20 \times 10^3 - 39.2T + 0.075T^2 \quad (D3)$$

$$b = -103 + 0.708T - 1.20 \times 10^{-3}T^2 \quad (D4)$$

$$c = 0.022 \quad (D5)$$

$$\alpha = 0.543 - 3.54 \times 10^{-3}T + 5.69 \times 10^{-6}T^2 \quad (D6)$$

Table D1. Values of Parameters for eq D1

coefficients	value
c_1	$-7.1734882 \times 10^{-1}$
c_2	1.5985379×10^{-4}
c_3	$-4.9286471 \times 10^{-7}$
c_4	$-2.7855285 \times 10^{-7}$
c_5	1.1877015×10^{-9}
c_6	−96.539512
c_7	4.4774938×10^{-1}
c_8	101.81078
c_9	5.3783879×10^{-6}

In eqs D2−D6, units of temperature (T) and pressure (p) are K and MPa, respectively.

AUTHOR INFORMATION

Corresponding Author

*Telephone: 519-888-4567, ext. 36157. E-mail: szendehb@uwaterloo.ca.

ACKNOWLEDGMENT

The authors are indebted to the Natural Sciences and Engineering Research Council of Canada (NSERC) for financial support.

NOMENCLATURE

Acronyms

EOS = equation of state

Variables

A = surface area of the droplet (m^2)
a, b, and c = arbitrary constants defined in the paper
C = concentration of CO_2 in brine (kg/m^3)
C_s = CO_2 concentrations at the droplet−liquid interface (kg/m^3)
C_∞ = CO_2 concentrations in brine (kg/m^3)
C_{L-V} = London−van der Waals constant
c_1, c_2, ..., c_9 = parameters for eq D1
cte = constant sign
D = pipe diameter (m)
$D_{CO_2-brine}$ = diffusivity of CO_2 in brine (m^2/s or cm^2/s)
D_{CO_2-W} = diffusivity of CO_2 in water (m^2/s or cm^2/s)
d_p = droplet (particle) diameter (m)
dm/dt = mass flux on droplet boundary (kg/s)
f = friction factor
f_{CO_2} = fugacity of CO_2 (Pa)
g = acceleration due to gravity (m/s^2)
$I \propto 5.3DRe_f^{-3/4}$ = inner turbulence scale (m)
K_H = Henry's constant
k = coefficient of mass transfer (m/s)
L = pipeline length (m)
M_w = molecular weight (kg/kmol)
m = mass (kg)
p = pressure (Pa or bar)
R_p = particle (droplet) radius (m)
R_{cell} = cell diameter (m)
$Re_p = Ud_b/\nu$ = Reynolds number based on the droplet diameter
$Re_f = UD/\nu$ = Reynolds number based on the pipe diameter
Ro = roughness of pipe (m)
r = spherical coordinate
S = salinity in weight percent (%)
$Sc = \nu/D$ = Schmidt number
$Sh = kd_p/D_{CO_2-brine}$ = Sherwood number
T = temperature (°C or K)
t = time (s)
t_{max} = residence time of the droplet in the pipeline (s)
U = average flow velocity (m/s)
V_p = CO_2 drop (or particle) volume (m^3)
V_{cell} = cell volume (m^3)
V_L = liquid volume in a cell (m^3)
$V_{CO_2}^{bp}$ = molar volume of CO_2 at normal boiling point ($cm^3/gmol$)
$We = \rho_{brine}U^2d_p/\sigma$ = Weber number
x = x axis
x_{CO_2} = mole fraction of CO_2

Greek Letters

α = salting-out coefficient
β = association parameter
Δ = difference operator
ε_0 = energy dissipation per unit mass in turbulent stream (m^2/s^3)
μ = dynamic viscosity (mPa s)
$\nu = \mu/\rho$ = kinematic viscosity of liquid (m^2/s)
ρ = density of fluid (kg/m^3)
ρ_p = density of the CO_2 droplet (kg/m^3)
ρ_{brine} = density of brine (kg/m^3)
σ = surface tension (N/m)
ϕ = CO_2 holdup
η = dissolution efficiency
$\propto$ = sign of proportionality

Subscripts

p = droplet (particle)
cell = drop cell
f = fluid
L = liquid
max = maximum
min = minimum
s = surface
W = water
0 = inlet (initial) pipe conditions

REFERENCES

(1) Halmann, M. M.; Steinberg, M. *Greenhouse Gas Carbon Dioxide Mitigation*; Lewis Publishers: Boca Raton, FL, 1999.

(2) Marchetti, C. *Climate Change* **1977**, *1*, 59.

(3) Intergovernmental Panel on Climate Change (IPCC). *IPCC: Special Report on Carbon Dioxide Capture and Storage*; IPCC: Geneva, Switzerland, 2005.

(4) Intergovernmental Panel on Climate Change (IPCC). *IPCC: The Physical Science Basis*; IPCC: Geneva, Switzerland, 2007.

(5) Malik, Q. M.; Islam, M. R. *Proceedings of the Society of Petroleum Engineers (SPE)/Department of Energy (DOE) Improved Oil Recovery Symposium*; Tulsa, OK, April 2000; SPE Paper 59327.

(6) Nordbotten, J. M.; Celia, M. A.; Bachu, S.; Dahle, H. K. *Environ. Sci. Technol.* **2005**, *39* (2), 602–611.

(7) Celia, M. A.; Nordbotten, J. M.; Bachu, S.; Dobossy, M.; Court, B. Risk of leakage versus depth of injection in geological storage. *Proceedings of the 9th International Conference on Greenhouse Gas Technologies (GHGT-9)*; Washington, D.C., Nov 2008.

(8) Celia, M. A.; Nordbotten, J. M. *Ground Water* **2009**, *47* (5), 627–638.

(9) Hassanzadeh, H.; Pooladi-Darvish, M.; Keith, D. W. *Transp. Porous Media* **2006**, *65*, 193–211.

(10) Leonenko, Y.; Keith, D. W. *Environ. Sci. Technol.* **2008**, *42*, 2742–2747.

(11) Vilarrasa, V.; Bolster, D.; Dentz, M.; Olivella, S.; Carrera, J. *Transp. Porous Media* **2010**, *85* (2), 619–639.

(12) Nordbotten, J. M.; Celia, M. A.; Bachu, S. *Transp. Porous Media* **2005**, *58*, 339–360.

(13) Dentz, M.; Tartakovsky, D. M. *Transp. Porous Media* **2009**, *79*, 15–27.

(14) Pau, G. S. H.; Bell, J. B.; Pruess, K.; Almgren, A. S.; Lijewski, M. J.; Zhang, K. *Adv. Water Resour.* **2010**, *33* (4), 443–455.

(15) Riaz, A.; Hesse, M. A.; Tchelepi, H. A.; Orr, F. M. *J. Fluid Mech.* **2006**, *548*, 87–111.

(16) Adams, J. J.; Bachu, S. *Geofluids* **2002**, *2* (4), 257–271.

(17) Hidalgo, J. J.; Carrera, J. *J. Fluid Mech.* **2009**, *640*, 441–452.
(18) Benson, S.; Myer, L. Monitoring to ensure safe and effective geologic sequestration of carbon dioxide. *Proceedings of the Intergovernmental Panel on Climate Change (IPCC) Workshop on Carbon Dioxide Capture and Storage*; Regina, Saskatchewan, Canada, 2002.
(19) Le Guern, F.; Sigvaldason, G. E. *J. Volcanol. Geotherm. Res.* **1989**, *39*, 95–276.
(20) Keith, D. W.; Giardina, J. A.; Morgan, M. G.; Wilson, E. J. *Environ. Sci. Technol.* **2005**, *39*, 499A–505A.
(21) Levich, V. G. *Physicochemical Hydrodynamics*; Prentice-Hall: Englewoods Cliffs, NJ, 1962.
(22) Clift, R.; Grace, J. R.; Weber, M. E. *Bubbles, Drops, and Particles*; Academic Press: New York, 1978.
(23) Nigmatulin, R. I. *Dynamics of Multiphase Media*; Hemisphere Publication Corporation: New York, 1991.
(24) Lezhnin, S.; Eskin, D.; Leonenko, Y.; Vinogradov, O. *Heat Mass Transfer* **2003**, *39*, 483–487.
(25) Kress, T. S.; Kyes, J. J. *Chem. Eng. Sci.* **1973**, *28*, 1809–1823.
(26) Ranz, W. E.; Marshall, W. R. *Chem. Eng. Prog.* **1952**, *48* (3), 141–146.
(27) Scott, D. S.; Hayduk, W. *Can. J. Chem. Eng.* **1966**, *44*, 130–136.
(28) Span, R.; Wagner, W. *J. Phys. Chem. Ref. Data* **1996**, *25*, 1509–1597.
(29) Spycher, N.; Pruess, K. *Geochim. Cosmochim. Acta* **2005**, *69* (13), 3309–3320.
(30) Spycher, N.; Pruess, K.; Ennis-King, J. *Geochim. Cosmochim. Acta* **2003**, *67*, 3015–3031.
(31) Rumpf, B.; Nicolaisen, H.; Ocal, C.; Maurer, G. *J. Solution Chem.* **1994**, *23*, 431–448.
(32) Duan, Z.; Sun, R. *Chem. Geol.* **2003**, *193* (3−4), 257–271.
(33) Duan, Z.; Sun, R.; Zhu, C.; Chou, I. *Mar. Chem.* **2006**, *98* (2−4), 131–139.
(34) Diamond, L.; Akinfiev, N. *Fluid Phase Equilib.* **2003**, *208*, 265–290.
(35) Johnson, M. T. *Ocean Sci. Discuss.* **2010**, *7*, 251–290.
(36) Teng, H.; Yamasaki, A. *J. Chem. Eng. Data* **1988**, *43*, 2–5.
(37) Bando, S.; Takemura, F.; Nishio, M.; Hihara, E.; Akai, M. *Chem. Eng. Data* **2003**, *48*, 576–579.
(38) Hibiki, T.; Goda, H.; Kim, S.; Ishii, M.; Uhle, J. *Int. J. Heat Mass Transfer* **2004**, *47*, 1847–1862.
(39) Angeli, P.; Hewitt, G. F. *Chem. Eng. Sci.* **2000**, *55*, 3133–3143.
(40) Thomas, R. M. *Int. J. Multiphase Flow* **1981**, *7*, 709–717.
(41) Chang, Y. B.; Coats, B. K.; Nolen, J. S. *SPE Reservoir Eval. Eng.* **1998**, *1* (2), 155–160.
(42) Hassanzadeh, H.; Pooladi-Darvish, M.; Elsharkawy, A. M.; Keith, D. W.; Leonenko, Y. *Int. J. Greenhouse Gas Control* **2008**, *2*, 65–77.
(43) McMillan, B. M.; Bryant, S. L. *Proceedings of the Society of Petroleum Engineers (SPE) Annual Technical Conference and Exhibition*; Anaheim, CA, Nov 2007.
(44) Haszeldine, R. S.; Quinn, O.; England, G.; Wilkinson, M.; Shipton, Z. K.; Evans, J. P.; Heath, J.; Crossey, L.; Ballentine, C. J.; Graham, C. M. *Oil Gas Sci. Technol.* **2005**, *60* (1), 33–49.
(45) Andre, L.; Audigane, P.; Azaroual, M.; Menjoz, A. *Energy Convers. Manage.* **2007**, *48*, 1782–1797.
(46) Audigane, P.; Oldenburg, C.; van der Meer, B.; Geel, C.; Lions, J.; Gaus, I.; Robelin, C. H.; Durst, P.; Xu, T. *American Association of Petroleum Geologists (AAPG) Special Publication on CO_2 Sequestration in Geological Media*; AAPG: Alexandria, VA, 2008.
(47) Gaus, I.; Audigane, P.; Andre, L.; Lions, J.; Jacquemet, N.; Durst, P.; Czernichowski-Lauriol, I.; Azaroul, M. *Int. J. Greenhouse Gas Control* **2008**, *2* (4), 605–625.
(48) Moore, J.; Adams, M.; Allis, R.; Lutz, S.; Rauzi, S. *Chem. Geol.* **2005**, *217* (3−4), 365–385.
(49) Cosham, A.; Eiber, R. *J. Pipeline Eng.* **2007**, *6* (3), 147–160.
(50) Steiner, R. *ASM Handbook*, 10th ed.; ASM International: Materials Park, OH, 2008.
(51) Rutqvist, J.; Birkholzer, J. T.; Cappa, F.; Tsang, C. F. *Energy Convers. Manage.* **2007**, *48*, 1798–1807.
(52) Ferronato, M.; Gambolati, G.; Janna, C.; Teatini, P. *Energy Convers. Manage.* **2010**, *51*, 1918–1928.
(53) Vilarrasa, V.; Bolster, D.; Olivella, S.; Carrera, J. *Int. J. Greenhouse Gas Control* **2010**, *4* (6), 910–919.
(54) Bell, J. S.; Price, P. R.; McLellan, P. J. *Geological Atlas of the Western Canada Sedimentary Basin*; Canadian Society of Petroleum Geologists and Alberta Research Council: Calgary, Alberta, Canada, 1994; Chapter 29.
(55) Green, D. W.; Perry, R. H. *Perry's Chemical Engineers' Handbook*, 8th ed.; McGraw-Hill: New York, 2008.
(56) Swamee, P. K.; Jain, A. K. *J. Hydraul. Eng.* **1976**, *102* (5), 657–664.
(57) Churchill, S. W. *Chem. Eng.* **1977**, *84*, 91.
(58) Chen, N. H. *Ind. Eng. Chem. Fundam.* **1979**, *18* (3), 296–297.
(59) Wilke, C. R.; Chang, P. *AICHE J.* **1995**, *1* , 264.
(60) Ratcliff, G. A.; Holdcroft, J. G. *Trans. Inst. Chem. Eng.* **1963**, *41*, 315–319.
(61) Al-Rawajfeh, A. E. Modelling and simulation of CO_2 release in multiple-effect distillers for seawater desalination. Ph.D. Dissertation, Department of Engineering Sciences, Institute of Thermal Process Engineering, Martin-Luther University of Halle-Wittenberg, Halle (Saale), Germany, 2004.
(62) Sayegh, S. G.; Najman, J. *Can. J. Chem. Eng.* **1987**, *65*, 314–320.
(63) Enick, R.; Klara, S. *Chem. Eng. Commun.* **1992**, *90*, 23–33.